Mass Transfer in Eddies Close to Air-Water Interface

Deterministic analyses applied to both velocity and concentration fluctuation data obtained in a region extremely close to air-water interface in a free-surface, unbaffled stirred tank allow estimation of the length and the velocity scales of individual eddies taking part in gas absorption. The mass transfer prediction by this method is superior to that by a statistical method using an integral length scale in the low-turbulence flow employed in this work. Eddy velocities are generally lower in the diffusion boundary layer zone compared with the bulk zone. Small eddies are generally associated with low velocity scales whereas large eddies occur at high velocity scales. Local mass transfer coefficients are high in regions where small eddies are dominant.

Sydney Luk, Y. H. Lee
Department of Chemical Engineering
Drexel University
Philadelphia, PA 19104

SCOPE

In earlier gas absorption models such as Higbie's (1935) penetration theory or Danckwerts' (1951) surface renewal theory, the fluid mechanics contribution is represented by a single parameter such as the exposure time or the surface renewal rate. In more recent models (Fortescue and Pearson, 1967; Lamont and Scott, 1970; Theofanous et al., 1976), attempts have been made to describe the convective diffusion in eddies near the gas-liquid interface in more realistic terms. These models contain statistically measurable length and velocity scales instead of a single parameter.

Experimentally, however, the investigation of mass transfer in individual eddies has not been possible. In the conventional method, the mean length and velocity scales are obtained independently from a sufficiently long data record of velocity fluctuations by using a suitable statistical method. These scales are then combined to give a single exposure time for the whole system. The major disadvantage of this approach is that in the process of the statistical averaging, the information on the length and velocity scales of individual eddies is lost. As a result, the eddy exposure time distribution cannot be obtained, the mass transfer predictions are often poor, and there is always a question as to which size eddy controls the mass transfer.

In the present study, we propose a direct analysis of the velocity or concentration fluctuation data by using a pseudosteady, two-dimensional single-eddy model to extract the length and velocity scales of individual eddies. This deterministic analysis readily enables estimations of the eddy exposure time distribution and the contribution of each eddy toward the overall mass transfer. The analysis is applied to both the velocity and concentration fluctuation data measured extremely close to the air-water interface in a free-surface, unbaffled stirred tank.

CONCLUSION AND SIGNIFICANCE

The predictions of mass transfer coefficients by deterministic analyses of both the velocity and concentration fluctuation data obtained at 90 μm depth from the air-water interface agree well with the experimental values obtained from local concentration profile measurements. The predictions by the statistical method employing the integral length scale are always lower due to underestimation of the length scale. The eddy

Correspondence concerning this paper should be addressed to Y. H. Lee.

velocity scales in the interfacial zone are lower than those in the liquid bulk, whereas the difference is not as significant with the eddy length scales.

In general, small eddies are associated with low velocity scales, and large eddies with high velocity scales. The local mass transfer coefficients are higher in locations where small eddies are dominant. The eddy exposure times obtained experimentally show a normal distribution skewed significantly toward the low exposure time side. This is in contrast to Danckwerts' age distribution function, which predicts unrealistically high distribution at zero age. The analysis is applied only to low-turbulence data due to experimental limitations. Whether the interpretation can be extended to higher turbulence data remains to be seen.

Experimental

Flow system

A schematic diagram of the flow system is shown in Figure 1. The absorption cell was a unbaffled Plexiglas tank (8 cm ID × 9 cm high) equipped with a magnetically driven impeller. The impeller was a 5.0 cm flat blade turbine with six equally spaced blades of 1.2 × 1 cm and was located 3.5 cm below the liquid surface.

A single impeller speed of 50 rpm (accurately maintained by a precision motor controller) was used throughout; this speed corresponds to an impeller Reynolds number of 2,083. Higher impeller speeds could not be used because of excessive ripples on the liquid surface. The absorption cell was placed on a vibration-free table so that the water surface was absolutely calm when there was no agitation. Approximately 300 mL of deoxygenated, 0.2 wt. % KCl in distilled water was used in all runs. The KCl was needed for concentration measurements. The temperature was maintained at 22 ± 1°C. Note that Figure 1 shows only the velocity measurement set-up. The concentration measurement set-up can be found elsewhere (Lee and Luk, 1982).

Velocity measurements

Velocities in the axial, tangential, and radial directions close to the gas-liquid interface were measured with a laser doppler anemometer (LDA) system (DISA Model 55L60) equipped with a frequency tracker and a flow direction adapter. To prevent light distortion due to tank wall curvature and to obtain a stronger signal, two flat optical lenses of approximately 2 cm dia. were installed opposite each other in the top part of the tank wall. The liquid level was maintained at about half the height of the optical lenses so that the laser beam (5 mW helium laser) could be directed extremely close to the gas-liquid interface. The seeding in the liquid was provided by adding 0.1 mL of homogenized milk per liter of distilled water. The LDA was used in the differential-Doppler, forward-scattering mode.

The tangential velocities were measured at two depths, 90 μm and 0.5 cm. The depths were estimated by:

1. Moving the laser beam as close as possible to the interface but not touching it.
2. Adding liquid with a syringe until a first signal was obtained.

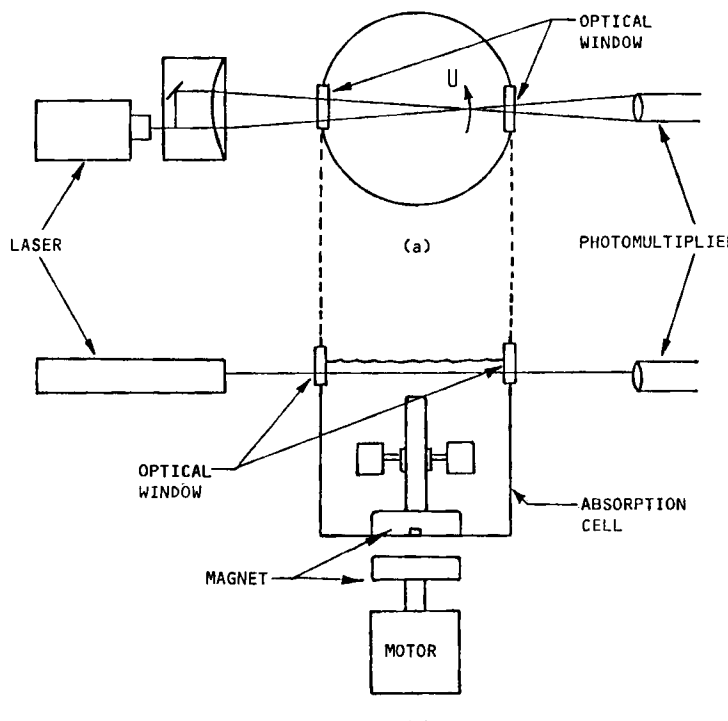

Figure 1. Flow system and velocity measurement set-up.

3. Adding a calculated volume of liquid to the vessel such that the desired depth is achieved.

Since the LDA measures velocities in a 160 × 422 μm football-shaped volume created by the intersecting laser beams, the uncertainty in the depth measurement was on the order of ±80 μm. To prevent evaporation of water, the vessel was covered during measurements.

The entire system was mounted on an optical bench and a milling machine table. This arrangement allowed the LDA system to be moved in three dimensions with an accuracy of ±0.2 mm. The absorption cell was mounted independently on a separate table. The voltage signal from the LDA system was acquired with a microcomputer equipped with an analog-to-digital converter. Details of the experimental setup and the data acquisition method are described elsewhere (Luk, 1984).

Concentration measurements

As oxygen was absorbed into the deoxygenated liquid, the local oxygen concentration fluctuations in the diffusion boundary layer were measured with an oxygen microprobe having a tip diameter on the order of 1 to 2 μm. Microprobes with a 95% response time of less than 10 ms were employed. The tip portion of the probe was gradually tapered so that the probe would not bend or vibrate when placed in an agitated liquid. A precision micromanipulator capable of moving in 2 μm steps was employed for positioning the microprobe.

When the probe was dipped in the liquid, a meniscus was always formed around the probe body at the surface due to a surface tension effect. Excessive meniscus formation was prevented by coating the probe tip with a polymer. For example, the height of the meniscus was approximately 30 μm when the probe was dipped 900 μm from the liquid surface. At this position, the radius of the probe body at the gas-liquid interface was approximately 50 μm. Since the immersed portion of the probe body in actual concentration measurements is extremely small, the probe is not likely to interfere with the local flow field. Details of the construction method are described elsewhere (Lee et al., 1978), as are the measurement procedures (Lee and Luk, 1982).

The microprobe was also used for determining experimentally the local mass transfer coefficients. The probe was positioned at various depths from the liquid surface, and the local concentrations were measured for a predetermined period of time. From the mean concentrations measured at different depths, a local concentration profile could be constructed. From the slope of the concentration profile at the interface, the local mass transfer coefficient could be estimated. Details of the methods for minimizing errors in depth measurements and for normalizing concentrations are given elsewhere (Lee and Luk, 1982).

A bulk oxygen probe (Nester Co., model 8000) was also used to measure the overall liquid film mass transfer coefficient k_L for the system by the dynamic method described by Dang et al. (1977).

Single-Eddy Model

The statistical approach based on the mean characteristic velocity and length scales, such as the root mean square velocity and the integral time scale, has been used widely in modeling gas absorption. However, this approach does not provide a detailed picture of the role the fluid mechanics of the individual eddies has on gas absorption. This is evidenced by a number of investigators (Fortescue and Pearson, 1967; Lamont and Scott, 1970; Theofanous et al., 1976; Davies and Lozano, 1979) trying to find which size eddy controls the mass transfer. The major disadvantage of the statistical approach is that in the process of averaging, the information on the length and velocity scales of individual eddies is lost. An alternative approach is to take into account the mass transfer contribution of each eddy taking part in gas absorption. This can be done by analyzing the velocity or concentration fluctuation data deterministically by using a suitable model for a single eddy.

Suppose a steady two-dimensional liquid eddy undergoes absorption while the liquid is convected, as shown in Figure 2a. Note that the two-dimensional assumption is valid only when the eddy is isotropic or when there is negligible z-component velocity. The latter applies in this case as shown by the velocity measurements given in the Results and Discussion section. The x-component velocity close to the interface u is zero at the two stagnant points ($x = 0$ and $x = L$), and reaches a maximum value at $x = L/2$, Figure 2b. Therefore, u can be approximated as:

$$u = V \sin\left(\frac{\pi x}{L}\right) \tag{1}$$

where V is the amplitude (referred to as the velocity scale henceforth).

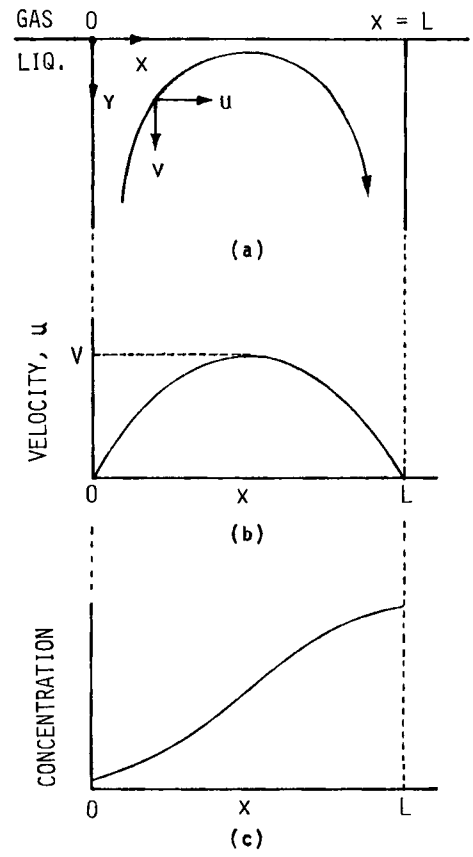

Figure 2. Eddy analysis.

a. Coordinate system used in single-eddy analysis
b. x-component velocity profile close to interface
c. Concentration profile close to interface

Suppose the concentration of the dissolved gas is measured as a function of x at a fixed depth from the interface. The concentration is expected to change as shown in Figure 2c. At the forward stagnation point ($x = 0$), the concentration is low because the liquid is coming up freshly from the bulk, whereas at the reverse stagnation point ($x = L$), the concentration is high due to absorption while the liquid is convected through a distance L. The concentration map of the eddy can be obtained by solving a two-dimensional convective diffusion equation:

$$u\frac{\partial c}{\partial x} + v\frac{\partial c}{\partial y} = D\left(\frac{\partial^2 c}{\partial x^2} + \frac{\partial^2 c}{\partial y^2}\right) \tag{2}$$

Note that a pseudosteady assumption is used here. This is based on the experimental observation (Luk, 1984) that the thickness of the local mean concentration boundary layer did not change appreciably during the period of absorption.

Since the concentration boundary layer is very thin (Lee and Luk, 1982), the x-direction diffusion term can be neglected compared with the y-direction term. Equation 2 can then be simplified to:

$$u\frac{\partial c}{\partial x} + v\frac{\partial c}{\partial y} = D\frac{\partial^2 c}{\partial y^2} \tag{3}$$

When L is much greater than the depth of penetration, it is reasonable to assume that the u profile shown in Figure 2b does not change appreciably with y in the interfacial region. Then, from the continuity equation:

$$v = -y\left(\frac{\partial u}{\partial x}\right) \tag{4}$$

and Eq. 2 can be rewritten as:

$$u\frac{\partial c}{\partial x} - y\frac{\partial u}{\partial x}\frac{\partial c}{\partial y} = D\frac{\partial^2 c}{\partial y^2} \tag{5}$$

The boundary conditions are:

$$c = c_b \quad \text{at } x = 0 \tag{6a}$$

$$c = c_s \quad \text{at } y = 0 \tag{6b}$$

$$c = c_b \quad \text{at } y = \infty \tag{6c}$$

A small penetration assumption was used in the last boundary condition, Eq. 6c. The solution to Eq. 5 with the velocity profile given by Eq. 1 is (Ruckenstein, 1968; Theofanous et al., 1976):

$$\frac{c - c_b}{c_s - c_b} = 1 - \text{erf}\left(\frac{y}{\delta}\right) \tag{7}$$

where

$$\delta = \frac{2}{\sqrt{\pi}}\sqrt{\frac{D}{V/L}}\left(1 + \cos\frac{\pi x}{L}\right)^{-1/2} \tag{8}$$

The local mass transfer coefficient k_L of the eddy can be obtained from the slope of the concentration profile at $y = 0$. The mean value of k_L for the single eddy can then be obtained from:

$$\bar{k}_L = \frac{1}{L}\int_0^L k_L dx = 0.9\sqrt{\frac{D}{L/V}} \tag{9}$$

Note that only the length scale L and the velocity fluctuation amplitude V are needed to determine $\bar{k}_L$ for a single eddy.

Analyses of Velocity and Concentration Data

Suppose that a train of different size eddies travels past a fixed measurement point located at a depth y_o from the interface, as shown in Figure 3a. Assume that alternate eddies change their directions of rotation. If the velocity is measured at the measuring point, it will fluctuate around a mean value U as shown in Figure 3b. Note that when the directions of U and u are identical, the x-component velocity will be greater than U, whereas when the directions are opposite, it will be less than U. If the concentration is measured at the same point, it will fluctuate as shown by the solid line in Figure 3c. The amplitude of the velocity and the corresponding concentration are related as shown in Figure 2. Note that the velocity and the concentration fluctuate at the same frequency.

Since the oxygen microprobe has a finite response time, the

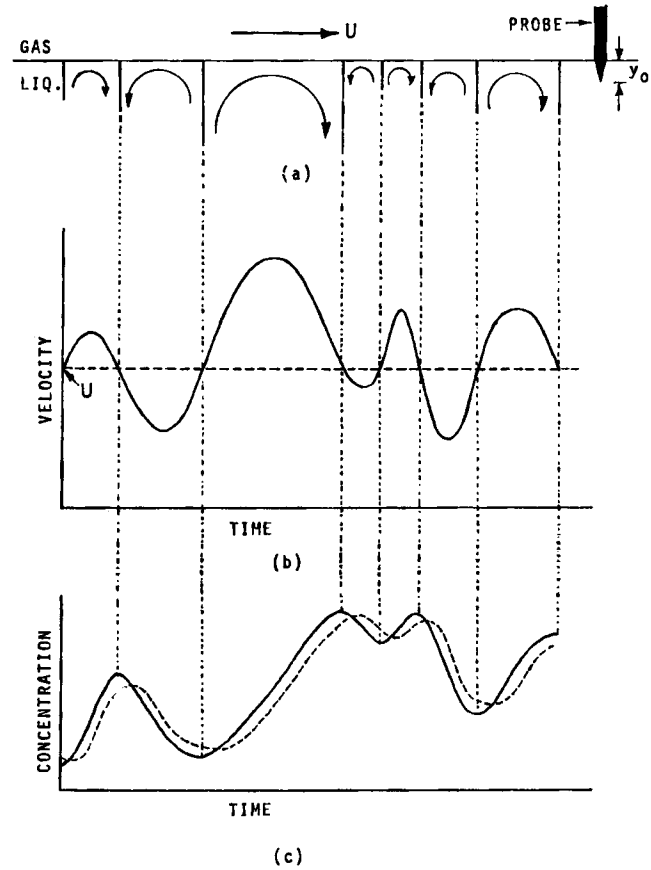

Figure 3. Analysis of eddies passing measurement point located at depth y_o.

a. Idealized eddies traveling at a mean velocity U
b. x-component velocity at measurement point
c. ——— concentration at measurement point
——— — concentration measured by microprobe

concentration actually measured by the probe will be somewhat damped and out of phase, as shown by the dotted line in Figure 3c.

Velocity data

In an unbaffled stirred tank equipped with a turbine impeller, the predominant flow is in the tangential direction. There is a weaker axial flow, and the two flow patterns generate eddies of different size and velocity. Since the radial velocity is negligibly small (Nagata et al., 1959), the tangential flow can be considered approximately two-dimensional at a fixed radial position. Therefore, the single-eddy model presented in Figure 2 can be applied to determine the length scale L_i and the velocity scale V_i of the ith eddy passing the measurement point after making proper changes in the coordinate system:

$$x = Ut \tag{10}$$

$$L_i = U\,t_i \tag{11}$$

$$V_i = \frac{\pi}{2}\,\bar{u}_i \tag{12}$$

where t_i is the time interval corresponding to a single eddy shown in Figures 3a and 3b, and $\bar{u}_i$ is the mean velocity of a single eddy:

$$\bar{u}_i = \frac{1}{t_i}\int_0^{t_i} u\,dt = \frac{1}{L_i}\int_0^{L_i} u\,dx \tag{13}$$

Although the single-eddy model employs a simplified sine profile for u, the real profile may be of irregular shape. In actual data analysis, the measured velocity u is numerically integrated according to Eq. 13 to obtain $\bar{u}_i$.

The average length and velocity scales are then calculated from:

$$\bar{L} = \frac{1}{N}\sum L_i \tag{14}$$

$$\bar{V} = \frac{1}{N}\sum V_i \tag{15}$$

and the average (L/V) by:

$$\overline{L/V} = \frac{1}{\Sigma t_i}\sum t_i(L/V)_i \tag{16}$$

Finally, the time-averaged local $\bar{k}_L$ at the measurement point is determined by:

$$k_{L,c} = \frac{1}{\Sigma t_i}\sum t_i(k_L)_i \tag{17}$$

where k_L for the ith eddy is calculated by Eq. 9.

The integral length scale L_I was also determined for comparison. An integral time scale t_I is obtained first by integrating the autocorrelation function $R(\tau)$:

$$R(\tau) = \frac{\overline{u(t)u(t+\tau)}}{\overline{u^2}} \tag{18}$$

and

$$t_I = \int_0^{t^*} R(\tau)\,d\tau \tag{19}$$

where t^* is the time when $R(\tau)$ first becomes zero. The $R(\tau)$ was computed from the digitized data via the fast Fourier transform method described by Bendat and Piersol (1971). The integral length scale is then calculated by:

$$L_I = U\,t_I \tag{20}$$

This method is essentially the same as that used for obtaining the Eulerian length scale of eddies (Hinze, 1959).

Concentration data

Since the oxygen microprobe shows a first-order response, the concentration measured by the probe, $g(t)$, can be expressed as:

$$g(t) = \int_0^t c(\tau)\exp\left(-(t-\tau)/k_p\right)d\tau \tag{21}$$

However, if the mean concentration of a single eddy is used for data analysis, the measured concentration can be used directly:

$$\bar{c}_i = \frac{1}{t_i}\int_0^{t_i} c(t)\,dt \approx \frac{1}{t_i}\int_0^{t_i} g(t)\,dt \tag{22}$$

where t_i is the time interval between the successive peak and valley. Since the probe response time was very short, the damping of the amplitude in each individual eddy was not significant except in very fast eddies.

A computer program was written to perform the following:

1. Calculation of the mean concentration $\bar{c}_i$ for each eddy as defined by Eq. 22.
2. Calculation of the L/V value from the solution of the single-eddy model that gives the same average concentration for a fixed depth y_o.
3. Calculation of the mass transfer coefficient of the eddy by Eq. 9.
4. Calculation of the cumulative average exposure time and the mass transfer coefficient by Eqs. 16 and 17, respectively.

The experimental local time-averaged k_L's were obtained from the measured local concentration profiles by:

$$(k_L)_{\text{local}} = -D\,\frac{1}{c_s - c_b}\left(\frac{\partial c}{\partial y}\right)_{y=0} \tag{23}$$

The corresponding exposure time was then determined by using Eq. 9. Note that in actual computations, the normalized concentration as given by the lefthand side of Eq. 7 was used throughout.

Results and Discussion

Flow patterns close to gas-liquid interface

The mean tangential velocities at depths of 90 μm and 0.5 cm are plotted in Figure 4 as a function of radial position. The mean tangential velocity is highest at a radial position 1.37 cm from the center ($r/R = 0.457$), which means that the radius of the central vortex zone is 1.37 cm (Nagata, 1975). Inside the central vortex zone U increases almost linearly with the radial posi-

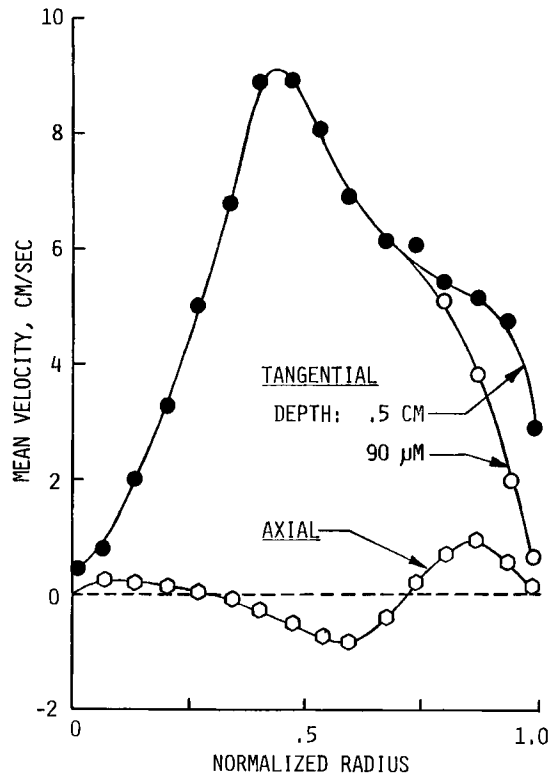

Figure 4. Changes in local mean tangential and axial velocities with radial positions.
Axial velocity obtained at 0.5 cm depth.

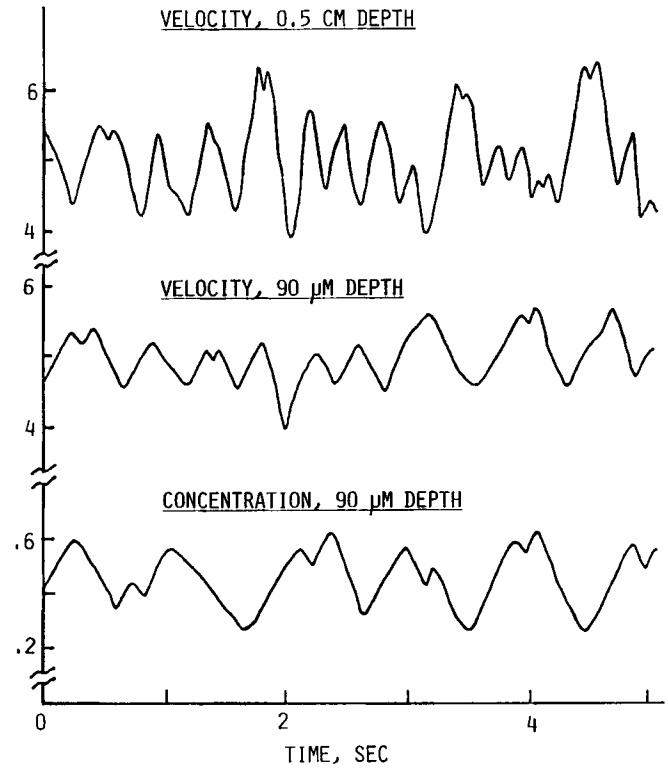

Figure 5. Velocity and normalized concentration fluctuations measured at $r/R = 0.8$.

tion, whereas outside the vortex zone U is roughly inversely proportional to r/R. The measured mean tangential velocity profile agrees well with the prediction given by Nagata.

The mean axial velocity at 0.5 cm depth is also plotted in Figure 4. The axial velocity is an order of magnitude smaller than the tangential velocity. Also, its flow direction changes. In the region close to the tank wall the flow is upward, whereas in the suction region on top of the turbine blades it is downward. It is interesting to note that the mean tangential velocity profile at 90 μm depth deviates from that at 0.5 cm starting at a position where the axial velocity becomes positive at $r/R = 0.72$. It appears that a strong interaction between the tangential and the axial flows is reponsible for the deviation.

The radial velocity was not easy to measure with the current set-up. We were able to measure it only at a single location: the average radial velocity was 0.05 cm/s at r/R of 0.17 and at a depth of 90 μm. Since the tangential velocity is dominant over the radial velocity, the flow can be considered approximately two-dimensional at a given radial position. This is in accordance with the assumption made in formulating the single-eddy model.

The velocity and concentration fluctuation data measured at $r/R = 0.8$ are shown in Figure 5. The velocity fluctuations measured at 0.5 cm depth show greater fluctuating amplitude and higher frequency compared with those at 90 μm depth. The concentration fluctuations measured at 90 μm depth show approximately the same frequency as the velocity fluctuations at the same depth, although the velocity fluctuations are slightly faster. Note that the LDA measures velocity in only one direction, whereas the concentration probe does not distinguish between directions. This similarity in fluctuation frequencies between the velocity and concentration confirms that the analysis presented in Figure 3 is reasonable.

Velocity scales

The eddy velocity scales calculated by Eq. 12 are shown in Figure 6. The velocity scales range between 5 and 76% of the mean velocity U shown in Figure 4, but the average is around 10%. The percentage figures are higher in both the center and the wall regions, where the mean velocities are lower. Also, note that the absolute velocity scales are smaller in these regions. Figure 6 clearly shows that the velocity scales in the boundary layer zone, i.e. at 90 μm depth, are significantly smaller than those in the liquid bulk. The scales at 90 μm depth are approximately 50 to 80% of those at 0.5 cm. In general, the retardation of velocity scales is more pronounced when the velocity scale itself is smaller. As pointed out by Davies (1972), the pressure force exerted by the eddies appears to be damped due to the counterbalancing capillary force at the interface. Note that it is not the mean velocity but the local eddy velocity that is retarded, and it is these eddies that renew the liquid surface.

In a stirred cell set-up, Davies and Lozano (1979) measured the root mean square fluctuating velocities of the tangential flow as a function of liquid depth with a hot-wire anemometer probe. They could measure the velocity as close as 500 μm depth from the liquid surface in high ranges of impeller Reynolds number (2,530 to 9,470). The measurements were only from a single radial position. They could not find a consistent trend in velocity reduction as the depth decreased. In a channel flow, Komori and Ueda (1982) showed that the streamwise and lateral velocities

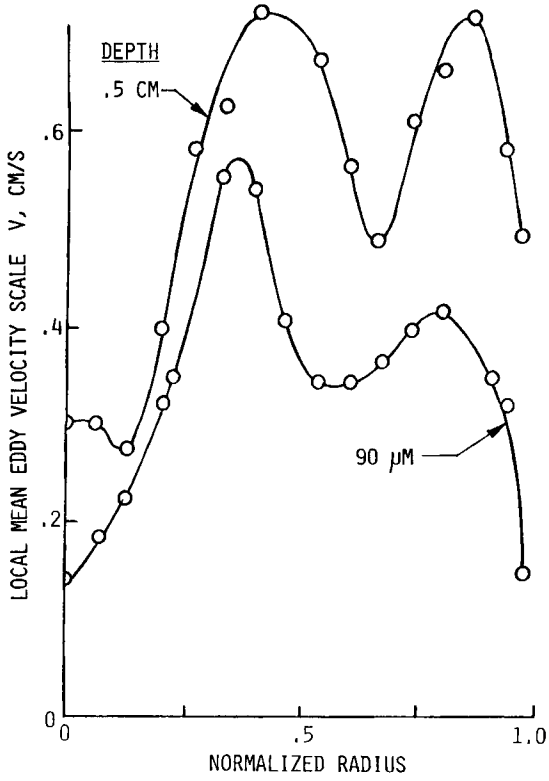

Figure 6. Changes in local mean eddy velocity scales obtained by Eq. 15 with radial position.

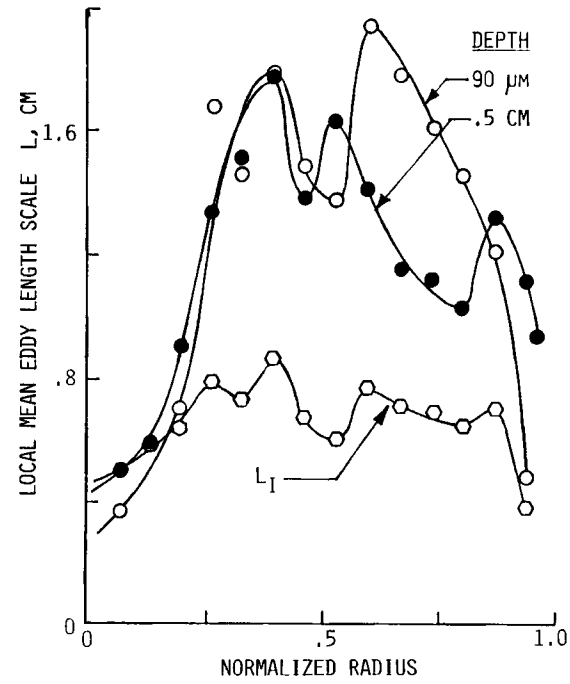

Figure 7. Changes in local mean eddy length scales obtained by Eq. 14 with radial position.

were promoted near the interface while the vertical velocity decreased. Our results, Figures 4 and 6, do not show such a trend.

Length scales

Figure 7 shows the length scales estimated by Eq. 14 from velocity fluctuation data obtained at depths 90 μm and 0.5 cm. Both length scales are close to each other in the region, $r/R <$ 0.5. In this region the shape of the length scale profile resembles that of the mean tangential velocity shown in Figure 4. However, in the region of major axial flow (where the mean axial velocity changes from a minimum to a maximum value as shown in Figure 4), the length scales at 90 μm depth are significantly higher than those at 0.5 cm. Note that the length scales in the downward flow region are higher than those in the upward flow region. In general, it appears that a high mean tangential velocity results in a large length scale, especially in a region where there is no significant secondary flow.

The integral length scales defined by Eq. 20 are also shown in Figure 7 for the velocity data obtained at 90 μm depth. In general, the shape of the profile is similar to the single-eddy model length scale, but the magnitudes are much smaller: less than half in most of the regions. Although the integral length scale has often been used in modeling gas absorption (Fortescue and Pearson, 1967; Theofanous et al., 1976; Davies and Lozano, 1979), its physical meaning is not clear. In contrast, the length scale employed in the present single-eddy model has a definite physical meaning. It is the length of the liquid element in the direction of the primary flow near the interfacial zone. It is interesting to note that if the velocity fluctuation is a pure sine wave, the integral length scale calculated by Eq. 20 is always smaller than the L shown in Figure 2. This may explain the observation that L_I is smaller than L.

The mean length scales shown in Figure 7 range between 0.4 and 2 cm. Davies and Lozano (1979) reported eddy integral length scales in the range of 5 to 9 mm, increasing with impeller Reynolds number. Their predictions of mass transfer coefficients by using the root mean square velocity and the integral length scale were much higher than their experimental measurements, especially when Re was low. Similar overpredictions were noted by Fortescue and Pearson (1967) in a channel flow when they used the integral length scale. These results suggest that the integral length scale may not represent the length scale that is responsible for mass transfer.

Exposure time and mass transfer

The term L/V in Eq. 9 is equivalent to the exposure time in Higbie's (1935) model or the reciprocal of the surface renewal rate in Danckwerts' (1951) model. Figure 8 shows L/V values obtained by five different methods. Except for the two profiles marked D and E, all other profiles show a similar pattern: the exposure time increases with r/R, reaches a maximum at r/R = 0.6, and then decreases almost linearly as the tank wall is approached. Note that the profile B, which was obtained from the measured mean local concentration gradients by Eq. 23, is considered as the experimentally measured exposure time. The predictions by the single-eddy model with velocity fluctuation data obtained at 90 μm depth, profile C, give slightly lower exposure times compared to the experimental profile B, whereas those obtained from concentration fluctuation data, profile A, give slightly higher exposure times. Since the actual flow may deviate from the two-dimensional behavior, the actual concentration gradients in eddies will be lower than those predicted by

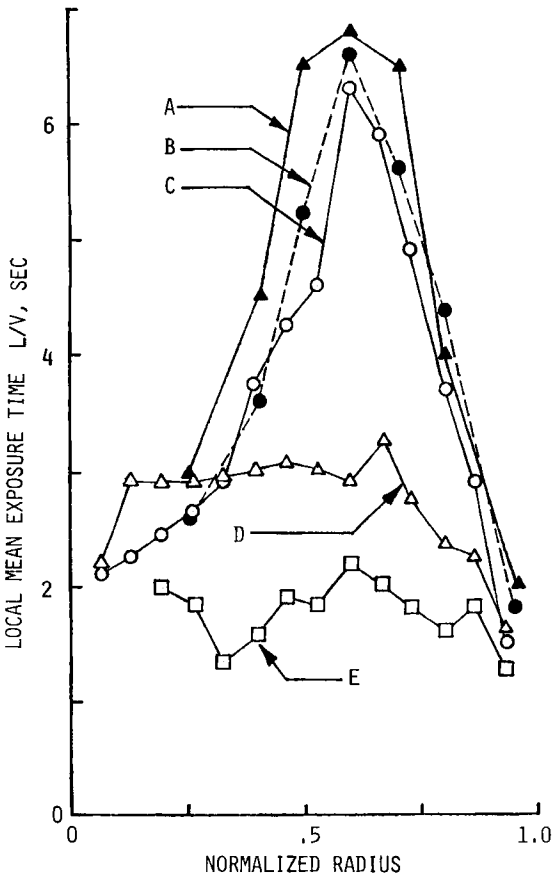

Figure 8. Comparisons of equivalent eddy exposure times.

A. Concentration fluctuation data at 90 μm depth
B. Local mean concentration profiles
C. Velocity fluctuation data at 90 μm depth
D. Velocity fluctuation data at 0.5 cm depth
E. Integral length scale and rms velocity

the two-dimensional model. The closeness of the profiles A and C to the profile B indicates that the two-dimensional and pseudosteady assumptions employed in the single-eddy model are reasonable.

The predictions by the single-eddy model with velocity data obtained at 0.5 cm depth, profile D, deviate significantly from profile C. This deviation is mainly due to the differences in length scales in the region where the axial flow is significant. The predictions by the integral length scale, profile E, show the lowest exposure times. This is expected because the estimated integral length scales are much lower than the eddy length scales in Figure 7.

It appears that when there is a significant secondary flow superimposed to the primary flow, (see Figure 4, $0.4 < r/R < 0.9$), both the velocity and the length scales differ significantly between the bulk (depth = 0.5 cm) and the interfacial zone (depth = 90 μm). Near the interface, the velocity scale decreases and the length scale increases (especially for $0.6 < r/R < 0.85$), and this results in an increase in exposure time. In general, small eddies are associated with low velocity scales, and large eddies with high velocity scales, Figures 6 and 7. However, small eddies are more efficient in terms of mass transfer because their exposure times are lower than those of the large eddies, Figures 7 and 8.

Note that the above comparison is only with the *mean scales* of L and V. In fact, there are distributions of scales in L and V. Figure 9 shows the distributions of exposure times obtained from velocity data at two radial positions. The shapes of the distribution curves are similar. They are skewed to the lower value. These experimental exposure time distributions can be compared with the age distribution function of Danckwerts (1952), which predicts an exponential decay. Realistically, however, it is not feasible to have a greater number of eddies with zero exposure time. Since both L and V are finite, the resulting exposure time has to be finite.

An independent measurement of the mass transfer coefficient by an oxygen electrode gave a mass transfer coefficient of 1.78×10^{-3} cm/s. This value compares favorably with the value of 1.94×10^{-3}, which was obtained by area-averaging the local mass transfer coefficients obtained by the local concentration profile measurements, profile B in Figure 8.

In the present single-eddy model, the measured velocity profile corresponding to a single eddy is fitted to a sine profile; see Eq. 12. This is in effect filtering out high-frequency components. However, the length scale distributions obtained experimentally are highest near the smallest scale, Figure 10. This means that although some high-frequency components are filtered, those in the vicinity of U are still taken into account.

The advantage of this deterministic approach is that the length scale of an eddy is combined with its own velocity scale for calculating the mass transfer contribution of the eddy; see Eqs. 16 and 17. However, in the statistical approach the length and velocity scales are obtained independently, and they are combined later for calculating the mass transfer coefficient. Therefore, the statistical approach is expected to make many mismatches between L's and V's on a single-eddy level. If the degree of the mismatch is considerable, then the prediction will deteriorate.

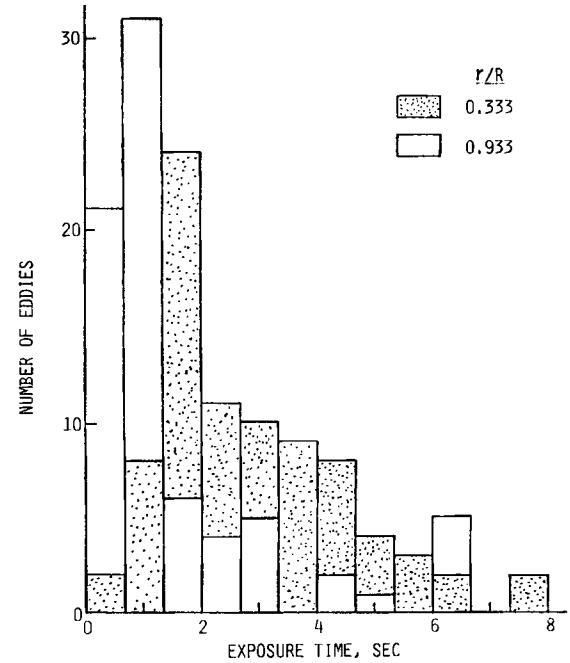

Figure 9. Exposure time distributions of eddies from velocity data obtained at 90 μm depth.

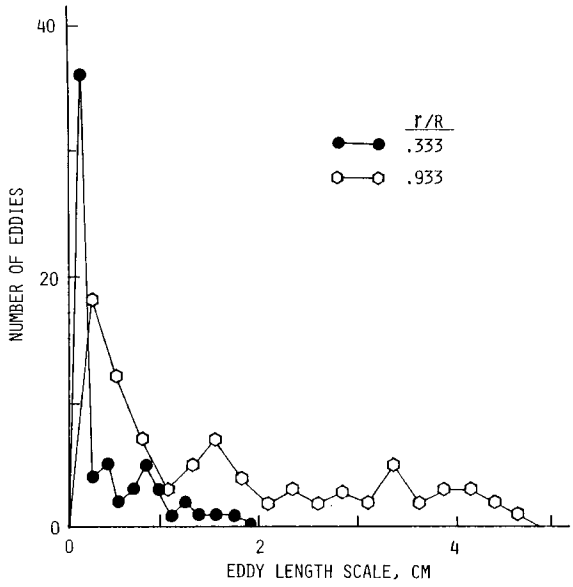

Figure 10. Length scale distributions of eddies from velocity data obtained at 90 μm depth.
For clarity, only midpoints of individual classes are shown.

Acknowledgment

We acknowledge the support of the National Science Foundation through Grant Nos. CPE 8101966 and CPE 8305356.

Notation

c = concentration, g/cm^3
c_b = bulk concentration, g/cm^3
c_s = concentration at interface, g/cm^3
$\bar{c}_i$ = mean concentration of ith eddy at a given depth, g/cm^3
D = diffusivity, cm^2/s
$g(t)$ = concentration as measured by probe, g/cm^3
$\underline{k}_L$ = liquid film mass transfer coefficient, cm/s
$\bar{k}_L$ = average mass transfer coefficient for an eddy, cm/s
$k_{L,c}$ = cumulative average k_L, cm/s
k_p = first-order time constant of microprobe, s
L = x-direction length scale of eddy, cm
L_I = integral length scale, cm
r = radial position, cm
R = radius of stirred cell, cm
$R(\tau)$ = autocorrelation coefficient
t = time, s
t_i = time period corresponding to a single eddy i, s
t_I = integral time scale, s
t^* = time when $R(\tau)$ first becomes zero, s
u = x-component eddy velocity close to interface, cm/s
U = average tangential velocity, cm/s
v = y-component eddy velocity close to interface, cm/s
V = amplitude of u (velocity scale of eddy), cm/s
x = distance along interface, cm
y = depth from interface, cm
y_o = depth of measurement, cm
δ = variable, Eq. 7
τ = time lag, s

Subscript

i = ith eddy

Symbols

$\bar{\ }$ = time-averaged value

Literature cited

Bendat, J. S., and A. G. Piersol, *Random Data—Analysis and Measurement Procedures*, Wiley-Interscience, New York (1971).

Danckwerts, P. V., "Significance of Liquid-Film Coefficients in Gas Absorption," *Ind. Eng. Chem.*, **43**, 1460 (1951).

Dang, N. D. P., D. A. Karrer, and I. J. Dunn, "Oxygen Transfer Coefficients by Dynamic Model Moment Analysis," *Biotech. Bioeng.*, **19**, 853 (1977).

Davies, J. T., "Turbulence Phenomena at Free Surfaces," *AIChE J.*, **18**, 169 (1972).

Davies, J. T., and F. J. Lozano, "Turbulent Characteristics and Mass Transfer at Air-Water Surfaces," *AIChE J.*, **25**, 405 (1979).

Fortescue, G. E., and J. R. A. Pearson, "On Gas Absorption into a Turbulent Liquid," *Chem. Eng. Sci.*, **22**, 1163 (1967).

Higbie, R., "The Rate of Absorption of a Pure Gas into a Still Liquid During Short Periods of Exposure," *Trans. Am. Inst. Chem. Engrs.*, **31**, 65 (1935).

Hinze, J. O., *Turbulence*, McGraw-Hill, New York (1959).

Komori, S., and H. Ueda, "Turbulence Structure and Transport Mechanism at the Free Surface in an Open Channel Flow," *Int. J. Heat Mass Transfer*, **25**, 513 (1982).

Lamont, J. C., and D. S. Scott, "An Eddy-Cell Model of Mass Transfer in the Surface of a Turbulent Liquid," *AIChE J.*, **16**, 513 (1970.)

Lee, Y. H., and S. Luk, "Characterization of Concentration Boundary Layer in Oxygen Absorption," *Ind. Eng. Chem. Fund.*, **21**, 428 (1982.)

Lee, Y. H., G. T. Tsao, and P. C. Wankat, "Ultramicroprobe Method for Investigating Mass Transfer through Gas-Liquid Interfaces," *Ind. Eng. Chem. Fund.*, **17**, 59 (1978).

Luk, S., "Mass Transfer in Eddies Close to Gas-Liquid Interface," Ph.D. Diss., Drexel Univ., Philadelphia, PA (1984).

Nagata, S., *Mixing Principles and Applications*, Wiley, New York (1975).

Nagata, A., Y. Yamamoto, and M. Ujihara, *Kagaku Kogaku* (Japanese), **23**, 130 (1959).

Ruckentstein, E., "A Generalized Penetration Theory for Unsteady Convective Mass Transfer," *Chem. Eng. Sci.*, **23**, 363 (1968).

Theofanous, T. G., R. N. Houze, and L. K. Brumfield, "Turbulent Mass Transfer at Free, Gas-Liquid Interfaces, with Applications to Open-Channel, Bubble, and Jet Flow," *Int. J. Heat Mass Transfer*, **19**, 613 (1976).

Manuscript received May 21, 1985, and revision received Jan. 8, 1986.